THE JOURNAL OF PHYSICAL CHEMISTRY A

Article

pubs.acs.org/JPCA

Electronic Absorption Spectra of Tetrapyrrole-Based Pigments via TD-DFT: A Reduced Orbital Space Study

Kushal Shrestha, Kyle A. Virgil, and Elena Jakubikova*

Department of Chemistry, North Carolina State University, Raleigh, North Carolina 27695, United States

Supporting Information

ABSTRACT: Tetrapyrrole-based pigments play a crucial role in photosynthesis as principal light absorbers in light-harvesting chemical systems. As such, accurate theoretical descriptions of the electronic absorption spectra of these pigments will aid in the proper description and understanding of the overall photophysics of photosynthesis. In this work, time-dependent density functional theory (TD-DFT) at the CAM-B3LYP/6-31G* level of theory is employed to produce the theoretical absorption spectra of several tetrapyrrole-based pigments. However, the application of TD-DFT to large systems with several hundreds of atoms can become computationally prohibitive. Therefore, in this study, TD-DFT calculations with reduced orbital spaces (ROSs) that exclude portions of occupied and virtual orbitals are pursued as a viable, computationally cost-effective alternative to conventional TD-DFT calculations. The effects of reducing orbital space size on theoretical spectra are qualitatively and quantitatively described, and both conventional and ROS results are benchmarked against experimental absorption spectra of various tetrapyrrole-based pigments. The orbital reduction approach is also applied to a large natural pigment assembly that comprises the principal light-absorbing component of the reaction center in purple bacteria. Overall, we find that TD-DFT calculations with proper and judicious orbital space reductions can adequately reproduce conventional, full orbital space, TD-DFT results of all pigments studied in this work.

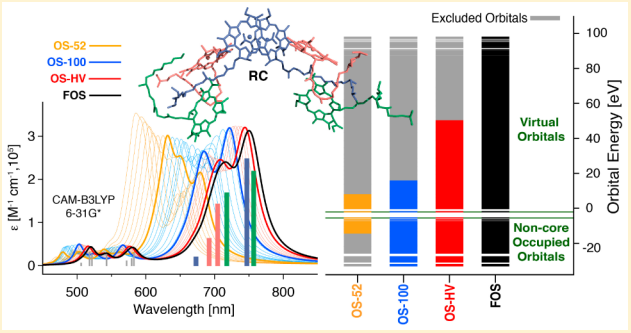

INTRODUCTION

Light absorption by tetrapyrrole-based pigments in plants and bacteria is an integral part of the natural photosynthetic process.[1] In photosynthetic organisms, these pigments are aggregated inside transmembrane, photosynthetic protein−pigment complexes,[2−4] and among the most extensively studied of these complexes are reaction centers of purple bacteria.[2,3,5−8] An accurate theoretical description of the light absorption process within photosynthetic complexes is vital to the overall understanding of natural photosynthesis.[9] Time-dependent density functional theory[10,11] (TD-DFT) is one of the approaches that can provide quantum chemical description of photoexcitations in protein-pigment complexes. Specifically, the linear-response formalism within TD-DFT can be used to predict excitation energies, absorption intensities, and excitation characteristics that can aid in spectral assignments.[12,13] However, the computational cost associated with TD-DFT increases rapidly with the size of the system, and the cost for calculating photoabsorption properties with TD-DFT becomes prohibitive for systems as large as photosynthetic proteins. For this reason, most theoretical studies involve TD-DFT calculations on simplified or reduced structural models of bacterial reaction centers.[14−16]

Despite drastic structural simplifications of the protein−pigment complexes to only essential light absorbing components consisting of thousands of atoms, TD-DFT calculations remain computationally demanding. Consequently, methodologies have been developed to reduce the computational cost of TD-DFT calculations for large systems by introducing different approximations to the underlying theory. For instance, subsystem density functional theory[17−19] and its time-dependent formalism[20] couples local subsystem excitations in a large system to produce the overall TD-DFT absorption spectrum.[21−24] Another set of approaches involves some form of reduction of the orbital space of Kohn−Sham (KS) TD-DFT.[25−30] TD-DFT with reduced orbital space has been successfully employed to compute X-ray absorption spectra,[28−30] absorption of explicitly solvated molecules,[26,27] and excited state molecular geometries.[25]

In this work, we adopt a reduced orbital space approach to TD-DFT calculations and investigate the effect of systematic orbital space reductions on the accuracy of TD-DFT results for tetrapyrrole-based systems, including the pigment assembly of the photosynthetic reaction center of purple bacteria. The goal is to assess the efficacy of reduced orbital space (ROS) approximations to TD-DFT results for the study of light absorption in tetrapyrrole-based pigments and pigment aggregates, in both natural and artificial systems.

Received: May 11, 2016
Revised: June 26, 2016
Published: July 8, 2016

DOI: 10.1021/acs.jpca.6b04797
J. Phys. Chem. A 2016, 120, 5816−5825

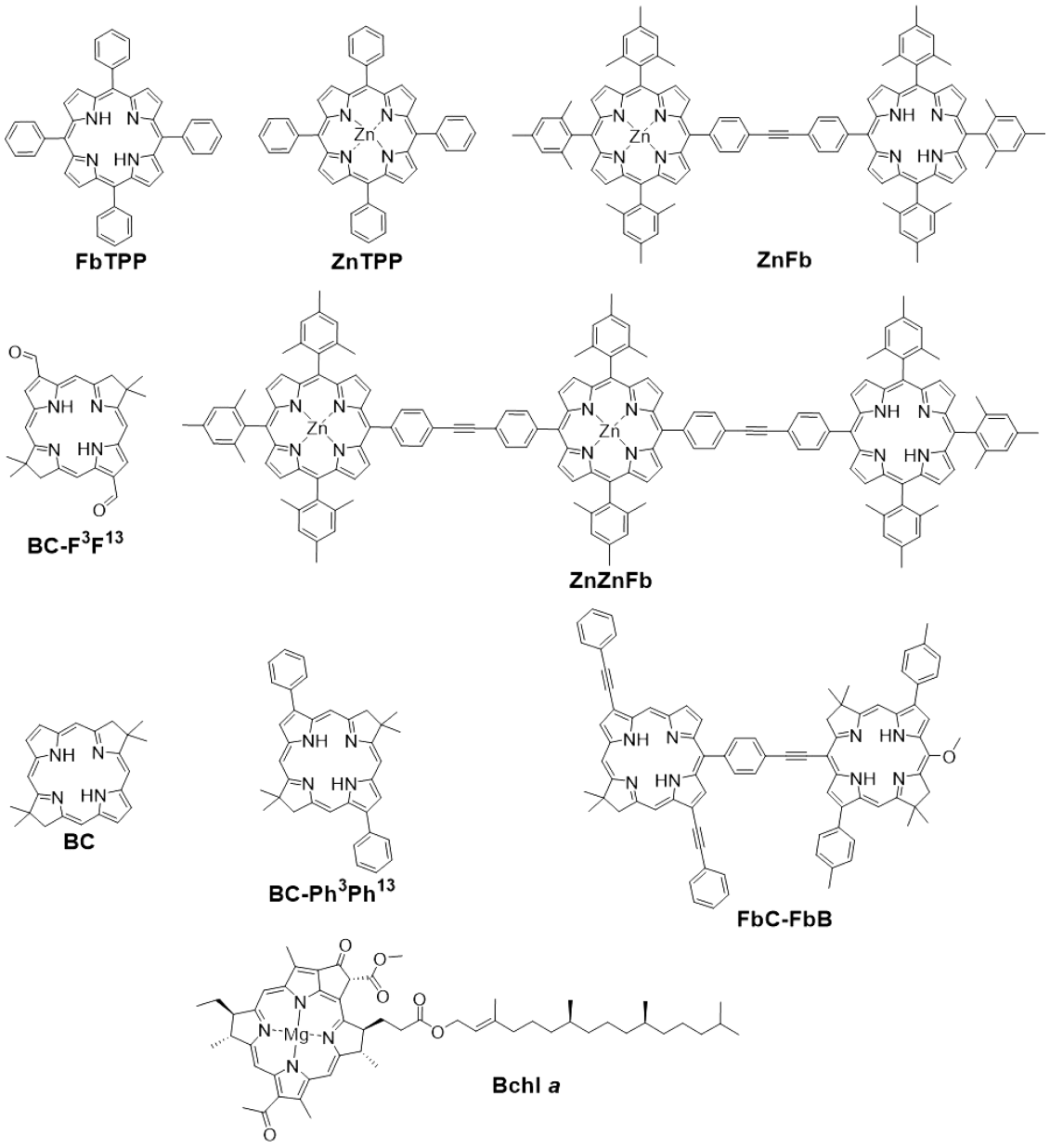

Figure 1. Tetrapyrrole-based benchmark systems.

The paper is organized as follows. First, electronic absorption spectra via ROS TD-DFT of benchmark tetrapyrrole-based systems (Figure 1) are acquired with orbital spaces of systematically decreasing sizes. Benchmark systems consist of the following tetrapyrrole-based molecules: three bacteriochlorin derivatives (BC, BC-F^3F^{13}, and BC-Ph^3Ph^{13}), bacteriochlorophyll *a* (Bchl *a*), free-base tetraphenylporphyrin (FbTPP), zinc tetraphenylporphyrin (ZnTPP), a chlorin−bacteriochlorin heterodimer (FbC-FbB), a zinc porphyrin and free-base porphyrin dimer (ZnFb), and an oligomer composed of two zinc porphyrin and one free-base porphyrin subunit (ZnZnFb). Unlike natural protein−pigment complexes, the benchmark systems listed above are structurally much simpler without complex protein environments. These simple artificial systems allow for direct comparison of calculated absorption spectra with experimental absorption spectra in solvent and, therefore, are well suited as benchmark systems. Finally, electronic absorption spectra via ROS TD-DFT and conventional TD-DFT are computed and results are discussed for the six-pigment cluster of the reaction center of *Rhodopseudomonas palustris*, which shall be referred to as RC from this point forward.

COMPUTATIONAL METHODS

The ground state structures of all monomers, dimers, and the trimer were optimized in a vacuum by employing the B3LYP functional.[31] The 6-31G* basis set[32−34] for C, H, N, O, Mg and the LANL08 effective core potentials with the associated basis set[35,36] for Zn were employed for all calculations. Excited state calculations via TD-DFT were performed using the CAM-B3LYP functional.[37] Although the B3LYP functional and the CAM-B3LYP functional both provide very similar absorption spectra for all monomeric benchmark systems, the CAM-B3LYP functional was chosen for all TD-DFT calculations in this work as the CAM-B3LYP functional provides a more accurate description of charge-transfer excitations in systems

DOI: 10.1021/acs.jpca.6b04797
J. Phys. Chem. A 2016, 120, 5816−5825

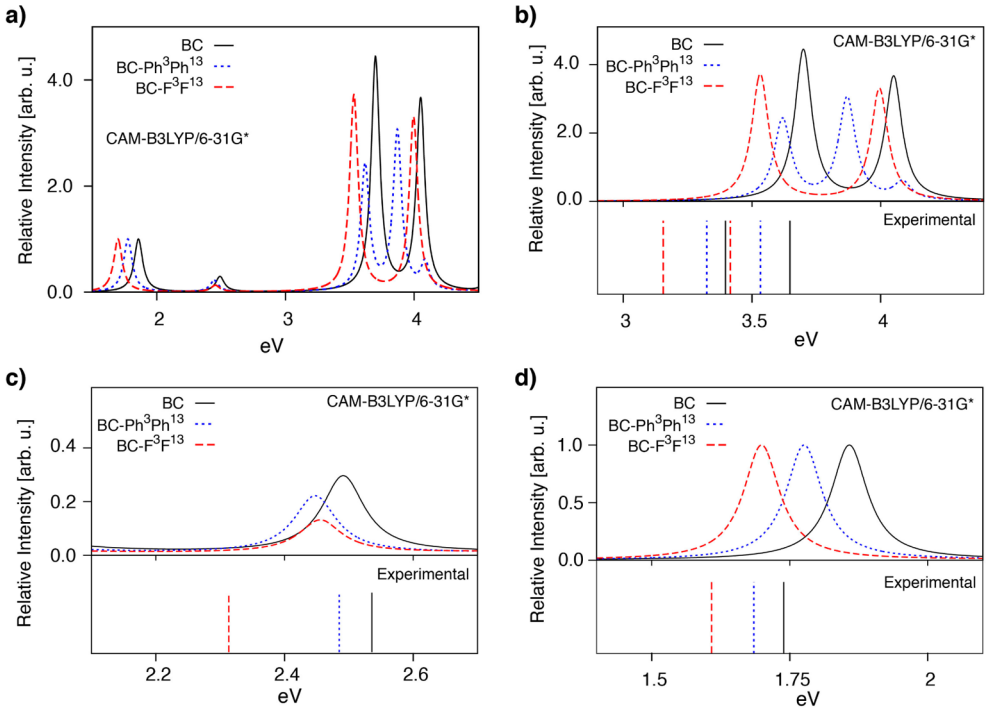

Figure 2. Calculated electronic absorption spectra (CAM-B3LYP/6-31G*) of BC (black solid line), BC-Ph^3Ph^{13} (blue dotted line), and BC-F^3F^{13} (red dashed-dotted line) along with energies of prominent experimental peaks (vertical lines) at four different energy ranges. The energy ranges cover the visible region (a), the Soret region (b), the Q_x region (c), and the Q_y region. Each spectrum is normalized to the lowest energy peak of its respective system.

with more than one tetrapyrrole-based pigment.[38,39] The 20 lowest energy, singlet excitations were computed for all systems in the study. Solvent was incorporated in TD-DFT calculations via the polarizable continuum model (PCM).[40] All TDDFT calculations for BC, BC-F^3F^{13}, BC-Ph^3Ph^{13}, ZnTPP, FbTPP, Bchl *a*, and FbC-FbB incorporated toluene as the solvent whereas TD-DFT calculations for ZnFb and ZnZnFb employed acetonitrile. The solvents in the TD-DFT calculations were chosen to match the solvents used in the experimental spectra of these systems. The PCM method was not employed in TD-DFT calculations involving RC.

Reduced orbital space TD-DFT calculations were performed for BC, BC-F^3F^{13}, BC-Ph^3Ph^{13}, ZnTPP, FbTPP, Bchl a, FbC-FbB, ZnFb, ZnZnFb, and RC. Throughout this work, the size of a given orbital space (OS) will be denoted as "OS-*N*" where *N* is equal to the percentage of the noncore occupied orbitals included in the OS with an equal number of virtual orbitals also included in the OS. The following reduced orbital spaces, using the "OS-*N*" labeling convention, were employed: OS-10, OS-20, OS-30, OS-40, OS-50, OS-60, OS-70, OS-80, OS-90, and OS-100. In addition, the orbital space denoted as "OS-HV" (where "HV" represents "Half-Virtual"), which includes all noncore occupied orbitals plus 50% of all virtual orbitals, and orbital space "FOS," which denotes the full orbital space that includes all noncore occupied orbitals plus all virtual orbitals, are also employed. All orbital spaces were constructed by selecting the proper number of occupied orbitals and virtual orbitals energetically closest to the highest occupied molecular orbital (HOMO) and the lowest unoccupied molecular orbital (LUMO), respectively (Figure S1). All calculations were performed using the Gaussian 09[41] (G09) software package. The orbital space size that is the default in G09 (Version B.01) for TD-DFT calculations is FOS. The simulated absorption spectra were derived from convoluting stick spectra with Lorentzian line functions over all excitation energies, each with a half-width-half-maximum of 0.04 eV.

The structure of RC was obtained from the crystal structure data with protein databank (PDB) code 1PYH.[42] For TD-DFT calculations of RC, the excited state total electron density, $\rho^{EX}(\vec{r})$, for a given state was obtained via the relaxed one-particle density matrix and the Z-vector approach as implemented in G09.[10,43,44] Thus, a difference density function, $\Delta\rho^{EX}(\vec{r})$, was obtained for a given excitation such that $\Delta\rho^{EX}(\vec{r}) = \rho^{EX}(\vec{r}) - \rho_0(\vec{r})$, where $\rho_0(\vec{r})$ is the ground state total electron density. The difference density functions, $\rho^{EX}(\vec{r})$, for excitations in RC were all discretized into a 1600 × 1600 × 2000 point grid in a 105.3 Å × 98.7 Å × 168.6 Å rectangular prism. The completeness with which the discretized grid points describe $\Delta\rho^{EX}(\vec{r})$ can be assessed by numerical integration of $\Delta\rho^{EX}(\vec{r})$ over $\vec{r}$, which should yield zero. Hence, the accuracy of the finite grid is indicated by the closeness of the numerically integrated value of $\Delta\rho^{EX}(\vec{r})$ to zero. For this reason, depictions of $\Delta\rho^{EX}(\vec{r})$ throughout this study are accompanied by values that result from the numerical integration of the discretized $\Delta\rho^{EX}(\vec{r})$.

The analysis with difference density functions provides a straightforward description of the spatial character of a given excitation. Such characterization for excitations in large, multipigment assemblies like RC can be elusive when relying on information derived from one-electron transitions between occupied and unoccupied orbital pairs that describe the transition density.[13] However, excited state analyses of the smaller benchmark systems in this study have been tabulated using these one-electron orbital transitions. In those tabulated data, the contribution of an occupied−unoccupied orbital pair to the transition density of an excitation was calculated in the

DOI: 10.1021/acs.jpca.6b04797
J. Phys. Chem. A 2016, 120, 5816−5825

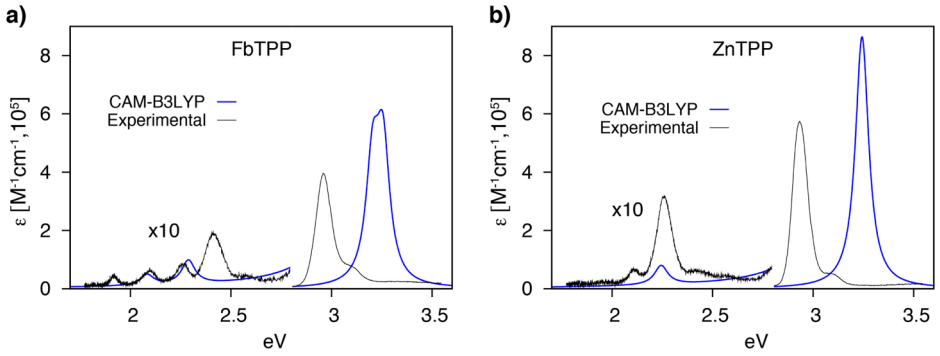

Figure 3. UV−vis absorption spectra of FbTPP (a) and ZnTPP (b). Experimental spectra[48] (solid black lines) in toluene are compared to calculated spectra (solid blue lines) at the CAM-B3LYP/6-31G* level of theory.

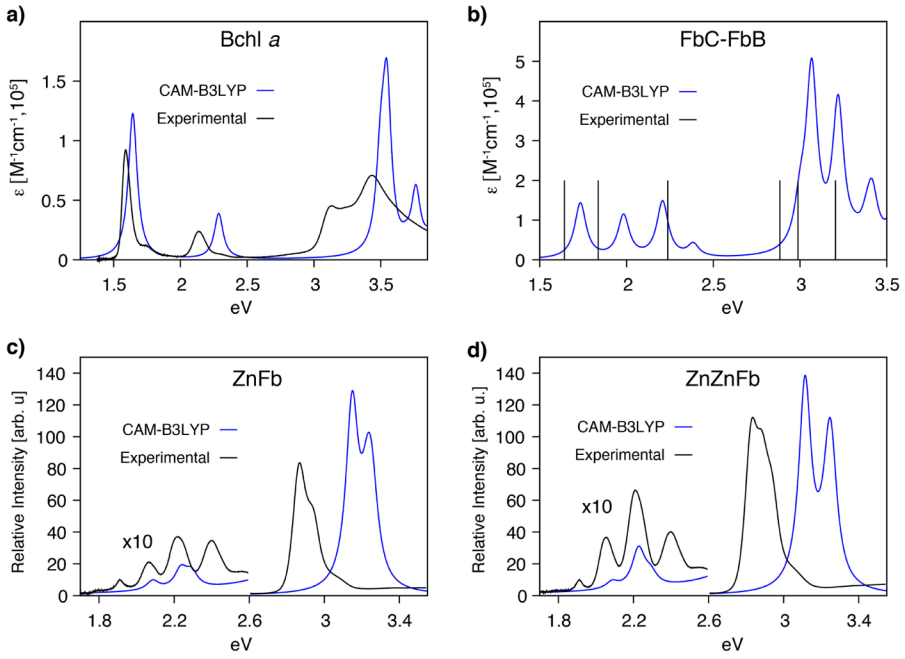

Figure 4. UV−vis absorption spectra of BChl *a* (a), FbC-FbB (b), ZnFb (c), and ZnZnFb (d). Experimental spectra[48−50] (solid black lines) are compared to calculated spectra (solid blue lines) at the CAM-B3LYP/6-31G* level of theory. Only excitation energies from the experimental peak maxima[49] (vertical black lines) are shown for FbC-FbB (b).

following way: $2(x_i^* x_i) \times 100\%$ and $-2(y_i^* y_i) \times 100\%$, where x_i and y_i are the components associated with occupied−unoccupied orbital pair i in the excitation solution vector, $\vec{X}$, and de-excitation solution vector, $\vec{Y}$, from the Casida equations, respectively.[45,46] This strategy for calculating the orbital transition contribution is attributable to the normalization conditions of the excitation and de-excitation solution vectors in the Casida equations.[13,45]

RESULTS AND DISCUSSION

In the sections that follow, electronic absorption spectra obtained via TD-DFT at the CAM-B3LYP/6-31G* level of theory for benchmark systems in Figure 1 and for RC are presented. After a comparison of the calculated absorption spectra of the benchmark systems with corresponding experimental spectra, the effects of reducing the orbital space in TD-DFT calculations are examined for all benchmark systems. Calculated absorption spectra employing reduced orbital spaces for RC are then examined and compared to the FOS TD-DFT absorption spectrum. Finally, an analysis of low-energy excitations of RC is provided along with spectral assignments of peaks in the absorption spectra at the CAM-B3LYP/6-31G* level of theory.

Comparison of Full Orbital Space TD-DFT Spectra with Experimental Spectra. Electronic absorption spectra for all benchmark systems shown in Figure 1 were computed at the CAM-B3LYP/6-31G* level of theory. Calculated electronic spectra for the bacteriochlorin monomers (BC, BC-Ph^{3}Ph^{13}, and BC-F^{3}F^{13}) are compared with experimental absorption spectra in Figure 2. The calculated spectra for BC, BC-Ph^{3}Ph^{13}, and BC-F^{3}F^{13} show four prominent absorption peaks, which is qualitatively in agreement with the experimental data[47] shown in Figure 2, where vertical lines represent prominent experimental peaks. The experimental trend[47] between the three bacteriochlorin monomers shows increasing blue shifts in the UV−vis absorption peaks as the molecule goes from BC to BC-Ph^{3}Ph^{13} to BC-F^{3}F^{13}. The CAM-B3LYP/6-31G* results reproduce this trend in two of the four prominent absorption peaks for each monomer. The trend is reproduced in the lowest energy peak, the Q_y peak, between 1.5 and 2 eV (Figure 2d) and in the first peak of the Soret band between 3.5 and 3.7 eV

DOI: 10.1021/acs.jpca.6b04797
J. Phys. Chem. A 2016, 120, 5816−5825

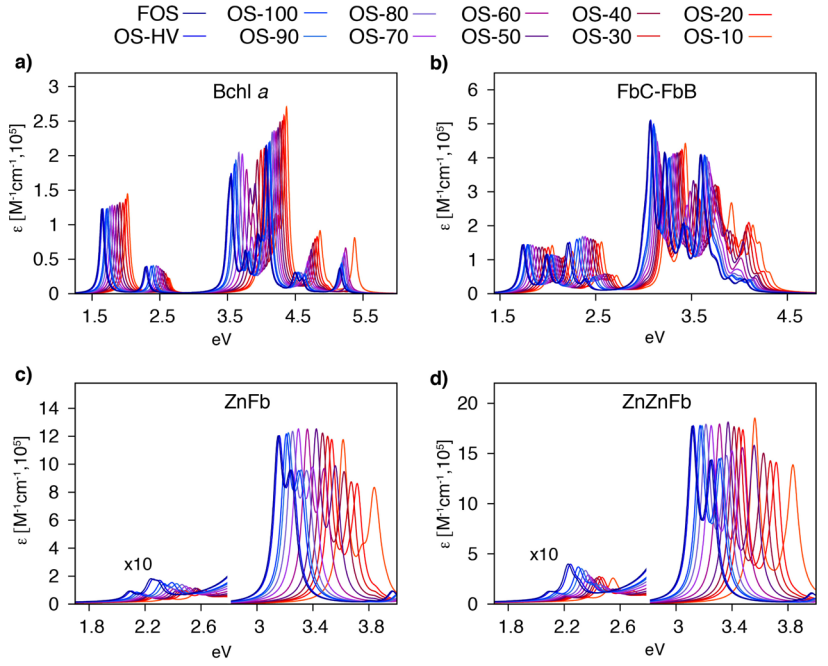

Figure 5. Calculated absorption spectra (20 excitations) for Bchl *a* (a), FbC-FbB (b), ZnFb (c), and ZnZnFb (d) resulting from the full orbital space and smaller orbital space. The orbital space size increases going from the red line ("OS-10" includes 10% of noncore occupied orbitals and an equal number of virtual orbitals) to the blue line ("FOS" includes all noncore occupied orbitals and all virtual orbitals).

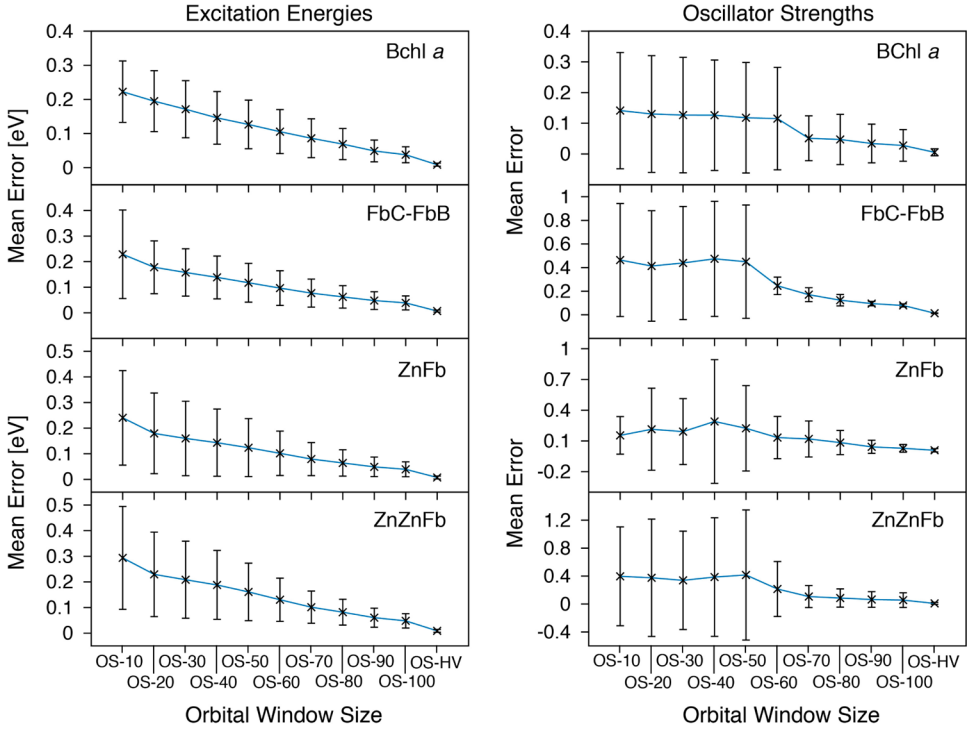

Figure 6. Average errors with standard deviations for the first 20 excitation energies and oscillator strengths of Bchl *a*, FbC-FbB, ZnFb, and ZnZnFb plotted with respect to orbital space size. The errors shown are derived from comparison with values from the FOS TD-DFT results.

(Figure 2b). The peak ordering in the Q_x region between 2.2 and 2.6 eV (Figure 2c) and also the second Soret peak region between 3.7 and 4.3 eV (Figure 2b) are reversed with respect to the experimental ordering for BC-Ph^{3}Ph[13] and BC-F^{3}F[13].

Comparison of calculated absorption and experimental spectra[48] of FbTPP and ZnTPP in Figure 3 shows that, similar to the BC monomer cases, the excitation energies are overestimated at the CAM-B3LYP/6-31G* level of theory. The absorption intensities in the Soret band between 3 and 3.5 eV are also overestimated, but the qualitative features of the FbTPP and ZnTPP spectra are reproduced. The calculated spectra contain two notable absorption bands, the Q (low energy) and the Soret (high energy) band. The Q-band for FbTPP contains two peaks. These features are in agreement with the experimental spectra. Note, however, that any vibronic progression present in the experimental spectra is not present

DOI: 10.1021/acs.jpca.6b04797
J. Phys. Chem. A 2016, 120, 5816−5825

in the calculated spectra as the nuclear positions are frozen in the calculations.

Similar comparisons are made between calculated spectra at the CAM-B3LYP/6-31G* level of theory and experimental spectra for Bchl *a*,[48] FbC-FbB,[49] ZnFb,[50] and ZnZnFb[50] in Figure 4. As with the porphyrin and bacteriochlorin monomers, the CAM-B3LYP functional reproduces the qualitative features of the UV−vis spectra of BChl *a*, FbC-FbB, ZnFb, and ZnZnFb but consistently overestimates the excitation energies. The intensity of the Soret bands for Bchl *a*, ZnFb, and ZnZnFb, which starts above 3 eV, is also overestimated by the functional (Figure 4a−d). Similar types of quantitative errors in excitation energies and intensities that are observed here have been assessed and previously observed in other studies.[51,52] Additionally, the use of smaller basis sets like 6-31G* has been shown to systematically overestimate excitation energies.[53]

The overall behavior of the CAM-B3LYP functional when excitation energies and intensities are computed for non-monomeric tetrapyrrole-based systems (FbC-FbB, ZnFb, ZnZnFb) does not deviate drastically from the behavior observed for the tetrapyrrole-based monomers in this study. For instance, the calculated spectra of the oligomers in Figure 4b−d do not show absorption features not present in the experiment. These results suggest that the CAM-B3LYP functional will reliably reproduce qualitative features of experimental absorption spectra for systems containing one or more tetrapyrroles with a systematic overestimation of excitation energies and Soret band intensities.

Reduced Orbital Space TD-DFT Calculations. Reduced orbital space TD-DFT calculations were performed for all benchmark systems shown in Figure 1. All calculated spectra generated from reduced orbital space TD-DFT calculations for BChl *a*, FbC-FbB, ZnFb, and ZnZnFb are shown in Figure 5. The results in Figure 5 indicate that orbital spaces smaller than the full orbital space (all noncore occupied orbital and all virtual orbitals corresponding to the conventional orbital size in TD-DFT calculations), produce absorption spectra that are blue-shifted with respect to conventional results. The degree to which a reduced orbital space spectrum is blue-shifted is directly related to the size of the orbital space. Note this trend in going from smaller orbital space sizes to larger orbital space sizes in Figure 5. The deviations of the absorption intensities in the smaller orbital spaces, when compared to the full orbital space results for BChl *a*, FbC-FbB, ZnFb, and ZnZnFb, are also systematically reduced as the orbital space size is increased. These observations pertaining to the effect of the orbital size on absorption spectrum are equally valid for the other five monomeric tetrapyrrole systems in this study (Figures S2 and S3 in the Supporting Information).

The observations apparent from Figure 5 are further quantified in Figure 6 that displays the average errors and standard deviations in the excitation energies (Figure 6, left panel) and the absorption intensities (Figure 6, right panel) for the first 20 excitations of Bchl *a*, FbC-FbB, ZnFb, and ZnZnFb at different orbital sizes. As the orbital space size increases, the average errors in both the excitation energies and oscillator strengths for Bchl *a*, FbC-FbB, ZnFb, and ZnZnFb decrease. The standard deviations in the average excitation energy error also decrease systematically with increasing orbital space size (Figure 6). Unlike the smooth behavior of the standard deviations in excitation energy errors with respect to orbital space size (Figure 6, left panel), the standard deviations in oscillator strength errors stay close to 1.0 oscillator strength unit for small orbital spaces. These standard deviations then abruptly begin to decrease after the orbital space exceeds OS-60 (Figure 6, right panel). Equivalent observations can be made for the average error and standard deviation in the excitation energies and the absorption intensities of the other five monomeric tetrapyrrole-based systems in this study (Figures S4 and S5 in the Supporting Information).

For all benchmark systems in the study except FbTPP, a systematic decrease in the standard deviation of the oscillator strength errors is only observed for orbital spaces larger than OS-60. These results suggest that orbital spaces smaller than OS-60 may produce oscillator strengths that deviate heavily from conventional, FOS TD-DFT results. When the orbital space consists of a 100% of noncore occupied orbitals and an equal number of virtual orbitals, OS-100, average errors in the excitation energies are within 0.05 ± 0.03 eV and average errors in the oscillator strengths are within 0.03 ± 0.05 for all benchmark systems. The magnitude of average errors and standard deviations in OS-100 are low and provide an acceptable approximation of the FOS TD-DFT results for all benchmark systems in this study (Figures 5, 6, S4, and S5).

The second largest orbital space with 100% of noncore occupied orbitals and 50% of all virtual orbitals, OS-HV, reproduces FOS TD-DFT results with a better accuracy than OS-100 (Figure 5, 6, S2−S5). However, orbital spaces larger than OS-100, such as OS-HV, come with a significant increase in the computational cost. Therefore, on the basis of the assessment of the quality of results from all ROS TD-DFT calculations on benchmark systems in Figure 1, OS-100 offers an adequate approximation of conventional, FOS TD-DFT results for tetrapyrrole-based systems when calculations with larger orbital space sizes become computationally prohibitive. Furthermore, results from OS-100 can adequately approximate conventional TD-DFT results regardless of any variation in the type of tetrapyrrole involved or even the number of tetrapyrroles involved in a given system (Figures 5, 6, S2−S5).

Calculations employing OS-100 show computational performance enhancements in terms of computation speedup when measured in CPU time (Figure 7). The speedup becomes apparent when the ratio of the CPU times of conventional, FOS, and ROS calculations (T_{FOS}/T_{ROS}) is plotted as a function of the system size measured in the number of electrons (Figure 7). Although the benefits of OS-100 in terms of computational performance is modest for benchmark systems with less than 500 electrons, the speedup in

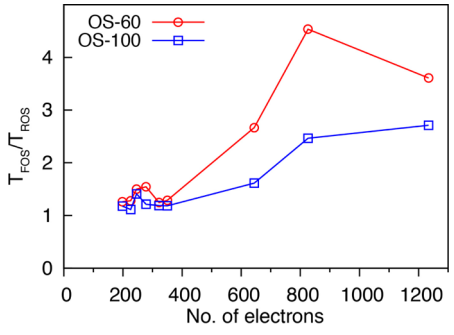

Figure 7. Timing ratio between CPU times for TD-DFT calculations with FOS and two reduced orbital spaces (T_{FOS}/T_{ROS}) for each benchmark system plotted against their respective number of electrons. Timing ratios for OS-60 and OS-100 are shown.

DOI: 10.1021/acs.jpca.6b04797
J. Phys. Chem. A 2016, 120, 5816−5825

computational processing more than doubles for benchmark systems that possess in excess of 1000 electrons (Figure 7), with the OS-100 TD-DFT calculation for ZnZnFb showing a speedup of 2.71. Finally, an examination and comparison of all OS-100 level excitations to the corresponding FOS level excitations in the Q-band energy region of the benchmark systems showed that the character of those excitations was not significantly altered by the reduction of the orbital space in OS-100. Side-by-side comparisons of OS-100 and FOS low-energy excitations are provided in Tables S1−S9 for each of the benchmark systems in Figure 1, and a close inspection of the orbital transitions that contribute to the transition density of a given excitation for a given benchmark molecule shows that the character of the excitation is mostly preserved in OS-100.

Although TD-DFT calculations with OS-100 are able to serve as reliable alternatives to conventional TD-DFT calculations for all benchmark systems in this study, very large tetrapyrrole-based pigment systems containing several pigments may pose an insurmountable computational barrier even with the reduction of the orbital space to OS-100. Further reduction of the orbital space for such large pigment assemblies may remain as the only viable option to obtain approximate TD-DFT absorption spectra. A smaller orbital space, OS-60, also showed tolerable average errors and standard deviations for excitations energies and especially for oscillator strengths for a majority of benchmark systems in this study (Figures S4, S5, and 6). Further analysis and comparison of the Q region from OS-60 with those from FOS shows that the character of such low-energy transitions remains mostly unchanged by the reduction of orbital space (Tables S10−S16). Note that OS-60 also showed improved computational speedup over OS-100, with the speedup from OS-60 for ZnZnFb equal to 3.6 (Figure 7). Therefore, OS-60 may be a viable option for very large, computationally challenging tetrapyrrole-based systems where qualitative descriptions of low-energy excitations are desired.

Reduced Orbital Space TD-DFT Spectra of RC. The results of the ROS TD-DFT calculations on RC (Figure 8) are presented in Figure 9, where Figure 9a compares absorption spectra from four ROS calculations to the conventional, FOS TD-DFT results. The spectra from smaller orbital spaces such as OS-24 and OS-52 provide quantitatively and qualitatively inaccurate approximations of the FOS TD-DFT spectrum. The OS-24, OS-52, and OS-62 results (Figure 9a) overestimate excitation energies and do not reproduce the relative intensities of the prominent absorption peaks. On the contrary, calculations with larger orbital spaces, as with OS-100 and OS-HV, reproduce the conventional, full orbital space absorption spectrum well (Figure 9a).

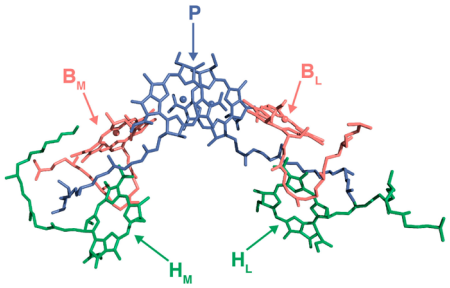

Figure 8. Structural representation of RC depicting the special pair of Bchl *a* pigments (labeled "P"), the accessory Bchl *a* pigments on the M polypeptide side (labeled "B_M") and on the L polypeptide side (labeled "B_L"), and the BPhe *a* pigments on the M side (labeled "H_M") and L side (labeled "H_L").[54]

The UV−vis spectrum afforded by OS-HV is an excellent approximation to the full orbital space UV−vis spectrum, but OS-HV demands significant computational resources as it requires 1425 more orbitals than OS-100, which utilizes a total of 2112 Kohn−Sham orbitals for RC. Moreover, results with OS-100 do not greatly deviate from the full orbital space results. Figure 9b quantifies average errors in the excitation energies and oscillator strengths with standard deviations for the first 20 excitations of RC, and it shows that, on average, the error in excitation energy and oscillator strength that is incurred upon using OS-100 is 0.04 ± 0.03 eV and 0.05 ± 0.06, respectively. Panels a and b of Figure 9 show that results from OS-100 are more approximate than those of OS-HV, but Figure 9 also clearly indicates that OS-100, which requires less computational resources than OS-HV, provides an acceptable and qualitatively accurate approximation of the conventional, FOS TD-DFT result.

Excited State Analysis for RC. Figure 10 shows isosurfaces of the excited state density difference function, $\Delta\rho^{EX}(\vec{r})$, associated with the first six excitations of RC at the CAM-B3LYP/6-31G* level of theory using the full orbital space. Because $\Delta\rho^{EX}(\vec{r})$ represents the change in the electron density of a many-electron system after an adiabatic vertical transition, inspection of the spatial distribution of this function for a given excitation yields insight into the character of that excitation. As such, each isosurface depicted in Figure 10 describes the extent of charge migration manifested by each of the six excitation events of RC. The majority of changes to the electron density for excitations that occur at 757, 718, 705, and 692 nm are localized on H_M, H_L, B_M, and B_L, respectively. Additionally, the spatial extent of $\Delta\rho^{EX}(\vec{r})$ for the seventh excitation at 583 nm is exclusively confined to H_L (Figure S6). However, excitations at 747 and 673 nm show appreciable changes in the electron density around both of the Bchl *a* pigments in the special pair, P (Figure 10). The delocalization of $\Delta\rho^{EX}(\vec{r})$ across P for these two excitations signal extensive electronic coupling of the pigments in P and imply that the two excitations comprise a strongly coupled excitonic pair.

The spectral assignments afforded by the analysis of $\Delta\rho^{EX}(\vec{r})$ for the low-energy transition of RC are summarized within the calculated spectrum shown in Figure 11 (bottom panel). As was the case for all of the tetrapyrrole-based benchmark calculations, the CAM-B3LYP/6-31G* absorption spectrum shown in Figure 11 is blue-shifted with respect to experimental peak positions[55] for the first absorption band (Figure 11, top panel). However, the CAM-B3LYP functional reproduces important qualitative features of the experimental absorption spectrum. In agreement with experiment, FOS TD-DFT with CAM-B3LYP yields two energetically separated absorption bands between 500 and 900 nm. In the calculated spectrum, the relative absorption intensity of the first absorption band is higher than that of the second absorption band (Figure 11), which also qualitatively agrees with the experimental[55] absorption profile. Nevertheless, the spectral assignments for the calculated peaks in the first absorption band (>600 nm) differ from established experimental assignments[3,54,56] where the 872, 801, and 750 nm absorption peaks are assigned to P, B, and H pigments, respectively (Figure 11, top panel). Furthermore, the results from TD-DFT in the first absorption band yield only two prominent peaks, whereas the experimental spectrum[55] shows three prominent peaks.

DOI: 10.1021/acs.jpca.6b04797
J. Phys. Chem. A 2016, 120, 5816−5825

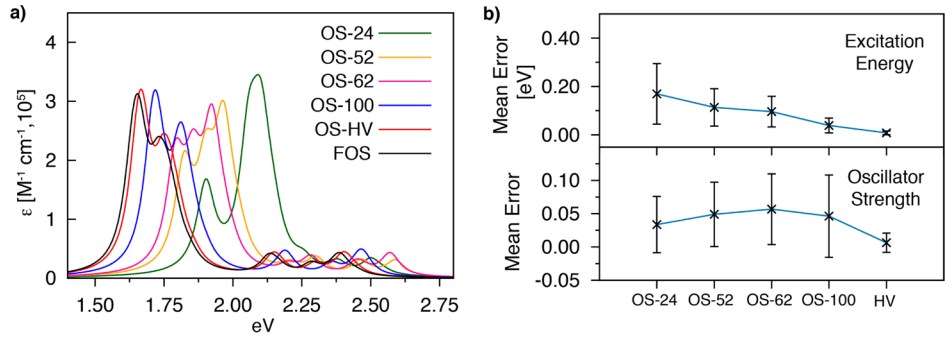

Figure 9. Calculated UV−vis absorption spectra (20 excitations) of RC using orbital spaces of five different sizes (a). Average errors with standard deviations for the first 20 excitation energies and oscillator strengths of RC are plotted with respect to orbital space size (b). The errors shown are derived from comparison with values from the FOS TD-DFT results.

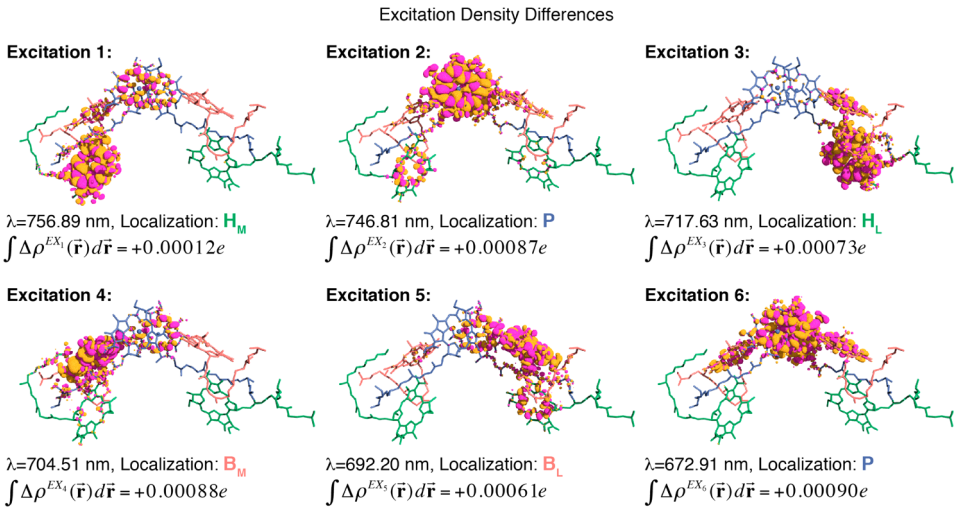

Figure 10. Positive (orange) and negative (pink) isosurfaces of the excitation density difference function, $\Delta\rho^{EX}(\vec{r})$, for the first six excitations of RC at the CAM-B3LYP/6-31G* level of theory with FOS TD-DFT. The integrated value of $\Delta\rho^{EX}(\vec{r})$ inside the isosurfaces shown is equal to 70% of the total integrated value of $\Delta\rho^{EX}(\vec{r})$, and the assignments to the different pigments of RC are labeled. The total numerical integral value of $\Delta\rho^{EX}(\vec{r})$ over all grid points are also shown, where e is the fundamental charge of the electron.

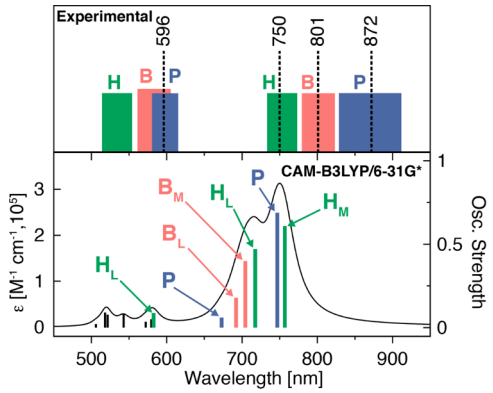

Figure 11. Electronic absorption spectrum at the CAM-B3LYP/6-31G* level of theory (FOS) of RC (bottom panel). Excitation wavelengths at absorption peak maxima of the experimental spectrum along with experimental assignments[3,54,56] to different pigments in RC (H, B, or P) (top panel, dashed lines for peak maxima, colored rectangles for peak assignments). Assignments at the CAM-B3LYP/6-31G* level of theory are also indicated for the seven lowest energy excitations (bottom panel). See also Figures 8, 10, and S6.

A previous computational study on the pigment assembly of the reaction center of *Rhodobacter sphaeroides* at the B3LYP/6-31G level of theory has been successful in generating an absorption spectrum with the correct number of peaks for the first absorption band with reasonable assignments.[15] The absorption spectrum obtained at the B3LYP/6-31G level is blue-shifted with respect to experimental peak positions and contains several zero intensity excitations with energies lower than those of the absorption peaks in the first absorption band,[15] which is indicative of dark states with possible charge-transfer character and underestimated excitation energies.[39] On the contrary, the lower absorption band of RC obtained at the CAM-B3LYP/6-31G* level is exclusively composed of the six excitations shown in Figures 10 and 11, with no dark states present (Figures 10 and 11). These six transitions represent multipigment excitons that very likely have their origins in the Q_y electronic transition of each of the six Bchl *a* pigments in RC. The shortcomings of the CAM-B3LYP/6-31G* results in Figure 11 may be related to the simplifications associated with the structural model of RC where the complex protein environment is excluded. Therefore, improved results may be accessible with the inclusion of protein residues closest to the RC pigments.

DOI: 10.1021/acs.jpca.6b04797
J. Phys. Chem. A 2016, 120, 5816−5825

CONCLUSIONS

In this study, results from ROS TD-DFT calculations of tetrapyrrole-based chemical were compared to results from conventional, FOS TD-DFT calculations at the CAM-B3LYP/6-31G* level of theory. The performance of the CAM-B3LYP functional for benchmark systems and RC was also evaluated by comparison with experimental absorption spectra. The main goal of this work was to investigate and clarify the impacts of reducing the orbital space in TD-DFT calculations involving tetrapyrrole-based systems. The conventional TD-DFT results with the CAM-B3LYP functional consistently overestimate excitation energies and Soret band intensities of benchmark tetrapyrrole-based systems, and the reduction of the orbital space in TD-DFT calculations further blue-shifts the calculated UV−vis spectra. Oscillator strengths begin to deviate significantly from the FOS results when the orbital space is smaller than that of OS-60. In this work, the CAM-B3LYP functional provides qualitatively accurate electronic absorption properties.

For all of the systems studied in this work, TD-DFT results with OS-100 provided acceptable and qualitatively accurate approximations of results from FOS TD-DFT calculations. Although OS-HV yielded results that were closest to those from FOS, OS-HV may not be computationally feasible for large systems. The effects of orbital space reductions on the calculated absorption spectra for RC were analogous to those observed for the tetrapyrrole-based benchmark systems, signifying that the impact of using reduced orbital spaces in TD-DFT calculations are transferrable between both natural and artificial tetrapyrrole-based pigments.

Difference density functions that result from excitations, $\Delta\rho^{EX}(\vec{r})$, were employed to simplify excited state analysis of multipigment assemblies, and analysis of these functions played a crucial role in the characterization of excitations in RC. The calculated spectrum and spectral assignments showed qualitative agreement with experiment and provided physical insight into the first absorption band of RC. Further improvement in the calculated spectrum of RC may hinge on the inclusion of the protein environment in the form of the amino acid residues closest to the pigments in the RC.

ASSOCIATED CONTENT

Supporting Information

The Supporting Information is available free of charge on the ACS Publications website at DOI: 10.1021/acs.jpca.6b04797.

Energy level diagram with different orbital spaces highlighted for FbC-FbB, TD-DFT absorption spectra with all orbital spaces for the five benchmark systems, plots of average errors with standard deviations in energies and intensities in all orbital spaces for the five benchmark systems, excitation density differences for RC with OS-100 and FOS, transition density analyses of Q region excitations with OS-100 and FOS for all benchmark systems, transition density analyses of Q region excitations with OS-60 and FOS for all benchmark systems (PDF)

AUTHOR INFORMATION

Corresponding Author

*E. Jakubikova. E-mail: ejakubi@ncsu.edu.

Notes

The authors declare no competing financial interest.

ACKNOWLEDGMENTS

This work was supported by the Department of Chemistry at North Carolina State University (NCSU) and used the resources of the High Performance Computing Center at NCSU. K. A. Virgil acknowledges support from the IMSD Scholars Program at NCSU supported by a NIH Grant 5-R25-GM083242. We gratefully acknowledge Prof. D. Holten (Washington University in St. Louis) for providing us with the experimental data of tetrapyrrole monomers and arrays used for comparison with our computational results.

REFERENCES

(1) Rabinowitch, E.; Govindjee, G. *Photosynthesis*; John Wiley & Sons, Inc.: New York, 1969.

(2) Hu, X.; Damjanović, A.; Ritz, T.; Schulten, K. Architecture and Mechanism of the Light-Harvesting Apparatus of Purple Bacteria. *Proc. Natl. Acad. Sci. U. S. A.* **1998**, *95*, 5935−5941.

(3) Jones, M. R. The Petite Purple Photosynthetic Powerpack. *Biochem. Soc. Trans.* **2009**, *37*, 400−407.

(4) Lancaster, C. R. D.; Ermler, U.; Michel, H. The Structures of Photosynthetic Reaction Centers from Purple Bacteria as Revealed by X-Ray Crystallography. In *Anoxygenic Photosynthetic Bacteria*; Blankenship, R. E., Madigan, M. T., Bauer, C. E., Eds.; Kluwer Academic Publishers: Dordrecht, The Netherlands, 1995; pp 503−526.

(5) Codgell, R. J.; Southall, J.; Gardiner, A. T.; Law, C. J.; Gall, A.; Roszak, A. W.; Isaacs, N. W. How Purple Photosynthetic Bacteria Harvest Solar Energy. *C. R. Chim.* **2006**, *9*, 201−206.

(6) Scholes, G. D.; Fleming, G. R.; Olaya-Castro, A.; van Grondelle, R. Lessons from Nature About Solar Light Harvesting. *Nat. Chem.* **2011**, *3*, 763−774.

(7) Pullerits, T.; Sundström, V. Photosynthetic Light-Harvesting Pigment−Protein Complexes: Toward Understanding How and Why. *Acc. Chem. Res.* **1996**, *29*, 381−389.

(8) Olson, T. L.; Williams, J. C.; Allen, J. P. The Three-Dimensional Structures of Bacterial Reaction Centers. *Photosynth. Res.* **2014**, *120*, 87−98.

(9) Blankenship, R. E. *Molecular Mechamisms of Photosynthesis*; Blackwell Science Ltd.: Great Britain, 2002.

(10) Furche, F.; Ahlrichs, R. Adiabatic Time-Dependent Density Functional Methods for Excited State Properties. *J. Chem. Phys.* **2002**, *117*, 7433−7447.

(11) Runge, E.; Gross, E. K. U. Density-Functional Theory for Time-Dependent Systems. *Phys. Rev. Lett.* **1984**, *52*, 997−1000.

(12) Casida, M. E.; Ipatov, A.; Cordova, F. *Lect. Notes Phys.* **2006**, *706*, 243−257.

(13) Casida, M. E. Time-Dependent Density-Functional Theory for Molecules and Molecular Solids. *J. Mol. Struct.: THEOCHEM* **2009**, *914*, 3−18.

(14) Linnanto, J.; Freiberg, A.; Korppi-Tommola, J. Quantum Chemical Simulations of Excited-State Absorption Spectra of Photosynthetic Bacterial Reaction Center and Antenna Complexes. *J. Phys. Chem. B* **2011**, *115*, 5536−5544.

(15) Ren, Y.; Ke, W.; Li, Y.; Feng, L.; Wan, J.; Xu, X. Understanding the Spectroscopic Properties of the Photosynthetic Reaction Center of Rhodobacter Sphaeroides by a Combined Theoretical Study of Absorption and Circular Dichroism Spectra. *J. Phys. Chem. B* **2009**, *113*, 10055−10058.

(16) Ren, Y.; Cheng, L.; Wan, J.; Li, Y.; Liu, J.; Yang, G.; Zhang, L.; Yang, S. A Theoretical Study of Electronic Excited States of Photosynthetic Reaction Center in Rhodopseudomonas Viridis. *Sci. China, Ser. B: Chem.* **2006**, *49*, 88−96.

(17) Govind, N.; Wang, Y. A.; Carter, E. A. Electronic-Structure Calculations by First-Principles Density-Based Embedding of Explicitly Correlated Systems. *J. Chem. Phys.* **1999**, *110*, 7677.

DOI: 10.1021/acs.jpca.6b04797
J. Phys. Chem. A 2016, 120, 5816−5825

(18) Wesolowski, T. A.; Warshel, A. Frozen Density Functional Approach for Ab Initio Calculations of Solvated Molecules. *J. Phys. Chem.* **1993**, *97*, 8050−8053.
(19) Hofener, S.; Gomes, A. S.; Visscher, L. Molecular Properties Via a Subsystem Density Functional Theory Formulation: A Common Framework for Electronic Embedding. *J. Chem. Phys.* **2012**, *136*, 044104.
(20) Khait, Y. G.; Hoffmann, M. R. Embedding Theory for Excited States. *J. Chem. Phys.* **2010**, *133*, 044107.
(21) Neugebauer, J. Couplings between Electronic Transitions in a Subsystem Formulation of Time-Dependent Density Functional Theory. *J. Chem. Phys.* **2007**, *126*, 134116.
(22) Pavanello, M. On the Subsystem Formulation of Linear-Response Time-Dependent DFT. *J. Chem. Phys.* **2013**, *138*, 204118.
(23) Neugebauer, J.; Curutchet, C.; Muñoz-Losa, A.; Mennucci, B. A Subsystem TDDFT Approach for Solvent Screening Effects on Excitation Energy Transfer Couplings. *J. Chem. Theory Comput.* **2010**, *6*, 1843−1851.
(24) Neugebauer, J. Subsystem-Based Theoretical Spectroscopy of Biomolecules and Biomolecular Assemblies. *ChemPhysChem* **2009**, *10*, 3148−3173.
(25) Robinson, D. Accurate Excited State Geometries within Reduced Subspace TDDFT/TDA. *J. Chem. Theory Comput.* **2014**, *10*, 5346−5352.
(26) Besley, N. A. Calculation of the Electronic Spectra of Molecules in Solution and on Surfaces. *Chem. Phys. Lett.* **2004**, *390*, 124−129.
(27) Liu, J.; Herbert, J. M. Local Excitation Approximations to Time-Dependent Density Functional Theory for Excitation Energies in Solution. *J. Chem. Theory Comput.* **2016**, *12*, 157−166.
(28) Stener, M.; Fronzoni, G.; de Simone, M. Time Dependent Density Functional Theory of Core Electrons Excitations. *Chem. Phys. Lett.* **2003**, *373*, 115−123.
(29) DeBeer George, S.; Petrenko, T.; Neese, F. Time-Dependent Density Functional Calculations of Ligand K-Edge X-Ray Absorption Spectra. *Inorg. Chim. Acta* **2008**, *361*, 965−972.
(30) Kozimor, S. A.; Yang, P.; Batista, E. R.; Boland, K. S.; Burns, C. J.; Clark, D. L.; Conradson, S. D.; Martin, R. L.; Wilkerson, M. P.; Wolfsberg, L. E. Trends in Covalency for D- and F-Element Metallocene Dichlorides Identified Using Chlorine K-Edge X-Ray Absorption Spectroscopy and Time-Dependent Density Functional Theory. *J. Am. Chem. Soc.* **2009**, *131*, 12125−12136.
(31) Becke, A. D. Density-Functional Thermochemistry. III. The Role of Exact Exchange. *J. Chem. Phys.* **1993**, *98*, 5648−5652.
(32) Hariharan, P. C.; Pople, J. A. The Influence of Polarization Functions on Molecular Orbital Hydrogenation Energies. *Theor. Chim. Acta* **1973**, *28*, 213−222.
(33) Hehre, W. J.; Ditchfield, R.; Pople, J. A. Self-Consistent Molecular Orbital Methods. XII. Further Extensions of Gaussian-Type Basis Sets for Use in Molecular Orbital Studies of Organic Molecules. *J. Chem. Phys.* **1972**, *56*, 2257−2261.
(34) Francl, M. M.; Pietro, W. J.; Hehre, W. J.; Binkley, J. S.; Gordon, M. S.; DeFrees, D. J.; Pople, J. A. Self-Consistent Molecular Orbital Methods. XXIII. A Polarization-Type Basis Set for Second-Row Elements. *J. Chem. Phys.* **1982**, *77*, 3654−3665.
(35) Wadt, W. R.; Hay, P. J. Ab Initio Effective Core Potentials for Molecular Calculations. Potentials for Main Group Elements Na to Bi. *J. Chem. Phys.* **1985**, *82*, 284−298.
(36) Roy, L. E.; Hay, P. J.; Martin, R. L. Revised Basis Sets for the LANL Effective Core Potentials. *J. Chem. Theory Comput.* **2008**, *4*, 1029−1031.
(37) Yanai, T.; Tew, D. P.; Handy, N. C. A New Hybrid Exchange−Correlation Functional Using the Coulomb-Attenuating Method (CAM-B3LYP). *Chem. Phys. Lett.* **2004**, *393*, 51−57.
(38) Kobayashi, R.; Amos, R. D. The Application of CAM-B3LYP to the Charge-Transfer Band Problem of the Zincbacteriochlorin−Bacteriochlorin Complex. *Chem. Phys. Lett.* **2006**, *420*, 106−109.
(39) Dreuw, A.; Head-Gordon, M. Failure of Time-Dependent Density Functional Theory for Long-Range Charge-Transfer Excited States: The Zincbacteriochlorin-Bacteriochlorin and Bacteriochlorophyll-Spheroidene Complexes. *J. Am. Chem. Soc.* **2004**, *126*, 4007−4016.
(40) Tomasi, J.; Mennucci, B.; Cammi, R. Quantum Mechanical Continuum Solvation Models. *Chem. Rev.* **2005**, *105*, 2999−3094.
(41) Frisch, M. J.; Trucks, G. W.; Schlegel, H. B.; Scuseria, G. E.; Robb, M. A.; Cheeseman, J. R.; Scalmani, G.; Barone, V.; Mennucci, B.; Petersson, G. A.; et al. *Gaussian 09*, Revision B.01; Gaussian Inc.: Wallingford, CT, 2009.
(42) Roszak, A. W.; Howard, T. D.; Southall, J.; Gardiner, A. T.; Law, C. J.; Isaacs, N. W.; Cogdell, R. J. Crystal Structure of the RC-LH1 Core Complex from Rhodopseudomonas Palustris. *Science* **2003**, *302*, 1969−1972.
(43) Handy, N. C.; Schaefer, H. F. On the Evaluation of Analytic Energy Derivatives for Correlated Wave Functions. *J. Chem. Phys.* **1984**, *81*, 5031−5033.
(44) Hansen, A. E.; Bouman, T. D. Optical Activity of Monoolefins: RPA Calculations and Extraction of the Mechanisms in Kirkwood's Theory. Application to (−)-Trans-Cyclooctene and 3(3R)-3-Methylcyclopentene. *J. Am. Chem. Soc.* **1985**, *107*, 4828−4839.
(45) Casida, M. E. Time-Dependent Density Functional Response Theory for Molecules. In *Recent Advances in Computational Chemistry*, 1st ed.; Chong, D. E., Ed.; World Scientific: Singapore, 1995; Vol. *1*, pp 155−192.
(46) Furche, F. On the Density Matrix Based Approach to Time-Dependent Density Functional Response Theory. *J. Chem. Phys.* **2001**, *114*, 5982.
(47) Taniguchi, M.; Cramer, D. L.; Bhise, A. D.; Kee, H. L.; Bocian, D. F.; Holten, D.; Lindsey, J. S. Accessing the near-Infrared Spectral Region with Stable, Synthetic, Wavelength-Tunable Bacteriochlorins. *New J. Chem.* **2008**, *32*, 947.
(48) Dixon, J. M.; Taniguchi, M.; Lindsey, J. S. Photochemcad 2: A Refined Program with Accompanying Spectral Databases for Photochemical Calculations. *Photochem. Photobiol.* **2005**, *81*, 212−213.
(49) Kee, H. L.; Diers, J. R.; Ptaszek, M.; Muthiah, C.; Fan, D.; Lindsey, J. S.; Bocian, D. F.; Holten, D. Chlorin-Bacteriochlorin Energy-Transfer Dyads as Prototypes for near-Infrared Molecular Imaging Probes: Controlling Charge-Transfer and Fluorescence Properties in Polar Media. *Photochem. Photobiol.* **2009**, *85*, 909−920.
(50) Song, H.-E.; Kirmaier, C.; Taniguchi, M.; Diers, J. R.; Bocian, D. F.; Lindsey, J. S.; Holten, D. Determination of Ground-State Hole-Transfer Rates between Equivalent Sites in Oxidized Multiporphyrin Arrays Using Time-Resolved Optical Spectroscopy. *J. Am. Chem. Soc.* **2008**, *130*, 15636−15648.
(51) Peach, M. J. G.; Helgaker, T.; Salek, P.; Keal, T. W.; Lutnaes, O. B.; Tozer, D. J.; Handy, N. C. Assessment of a Coulomb-Attenuated Exchange-Correlation Energy Functional. *Phys. Chem. Chem. Phys.* **2006**, *8*, 558−562.
(52) Baer, R.; Livshits, E.; Salzner, U. Tuned Range-Separated Hybrids in Density Functional Theory. *Annu. Rev. Phys. Chem.* **2010**, *61*, 85−109.
(53) Furche, F.; Rappoport, D. Density Functional Methods for Excited States: Equilibrium Structure and Electronic Spectra. In *Computational Photochemistry*; Olivucci, M., Ed.; Theoretical and Computational Chemistry; Elsevier: Amsterdam, 2005; Vol. *16*, pp 93−128.
(54) Zinth, W.; Wachtveitl, J. The First Picoseconds in Bacterial Photosynthesis - Ultrafast Electron Transfer for the Efficient Conversion of Light Energy. *ChemPhysChem* **2005**, *6*, 871−880.
(55) Mizoguchi, T.; Isaji, M.; Harada, J.; Tamiaki, H. Isolation and Pigment Composition of the Reaction Centers from Purple Photosynthetic Bacterium Rhodopseudomonas Palustris Species. *Biochim. Biophys. Acta, Bioenerg.* **2012**, *1817*, 395−400.
(56) Reed, D. W.; Ke, B. Spectral Properties of Reaction Center Preparations from Rhodopseudomonas Spheroides. *J. Biol. Chem.* **1973**, *248*, 3041−3045.

DOI: 10.1021/acs.jpca.6b04797
J. Phys. Chem. A 2016, 120, 5816−5825